Available online at www.sciencedirect.com
SCIENCE DIRECT®
International Journal of Heat and Mass Transfer 49 (2006) 3819–3830
International Journal of HEAT and MASS TRANSFER
www.elsevier.com/locate/ijhmt

Optimal active cooling performance of metallic sandwich panels with prismatic cores

L. Valdevit [a,*], A. Pantano [b], H.A. Stone [a], A.G. Evans [c]

[a] Div. of Eng. and Applied Sciences, Harvard University, Cambridge, MA 02138, USA
[b] Space Engineering SpA, Rome, Italy
[c] Materials Department, University of California, Santa Barbara, CA 93106, USA

Received 28 April 2005; received in revised form 24 February 2006
Available online 27 June 2006

Abstract

All-metallic sandwich panels with prismatic cores are being currently investigated for combined structural and active cooling performance. We present a new approach to active cooling performance, and use it to optimize the panel geometry for four different systems: aluminum-air, aluminum-water, aluminum-gasoline and titanium-gasoline. The results show that some geometric parameters can be fixed without much detriment in thermal performance. Moreover, while optimal core densities are typically 25–50%, near-optimal results can be obtained with densities as low as 10%. These findings provide considerable geometric flexibility when attempting combined thermal and structural optimization.

Keywords: Active cooling; Sandwich panels; Prismatic cores; Thermo-structural optimization; Genetic algorithm; Multi-functionality

1. Introduction

All-metallic sandwich panels with prismatic cores (Fig. 1a) are among the most weight-efficient structures, provided that the loading is parallel to the corrugation direction [1,2]. Concomitantly, their open core topology renders them amenable to active cooling: a fluid flowing through the open channels is capable of removing a heat flux impinging on one (or both) faces [3]. These designs might be suitable for many (aerospace and naval) applications, which require the simultaneous ability to sustain high heat flux while supporting large pressure or structural loads. With this bi-functionality in mind, the remaining challenge is to optimize the geometric parameters applicable to various combinations of structural and thermal loads. Structural optimization has been extensively addressed [4–7]. Moreover, analytic models and numerical studies exist for the overall heat transfer coefficient for panels with various core topologies, including foam [8,9], truss [10–13], textile [14,15] and honeycomb [16,17] cores. The latter have been reviewed [3] in an attempt to provide guidelines for *ranking* various heat sink technologies. However, the authors are unaware of attempts at *geometric optimization*. Here we address this deficiency for prismatic panels, with emphasis on corrugated and diamond cores. Initially, active cooling performance is defined in a way most useful for design. Two non-dimensional parameters are introduced, related to the achievable heat flux removal and the imposed pumping power. The panel geometry is then optimized with the goal of maximizing the heat flux at different values of pumping power.

The article is organized as follows. Section 2 relates this research with a previously published review [3]. Section 3 emphasizes the limitation of the previous approach and justifies the introduction of the new scheme. In Section 4, the new non-dimensional parameters are expressed as functions of the panel geometry and the material properties. Correlations are used to express the heat transfer and fluid flow performance at the duct level. While a similar

* Corresponding author. Tel.: +1 857 998 0578; fax: +1 617 496 0601.
E-mail address: lorenzo@engineering.ucsb.edu (L. Valdevit).

0017-9310/$ - see front matter © 2006 Elsevier Ltd. All rights reserved.
doi:10.1016/j.ijheatmasstransfer.2006.03.042

Nomenclature

c_p	specific heat (J/kg K)
D	hydraulic diameter (m)
H_c	core thickness (m)
h	heat transfer coefficient (W/m^2 K)
k	thermal conductivity (W/m K)
L	panel length (m)
m	inverse length-scale (m^{-1})
$\dot{m}$	flow rate (kg/s)
n	order of corrugation
p	pressure (Pa)
P	pumping Power (W)
q	specific heat flux (W/m^2)
Q	heat flux (W)
R	thermal resistance ((W/K)$^{-1}$)
t	core web thickness (m)
T	temperature (K)
u	flow velocity (m/s)
W	panel width (m)
x, y, z	cartesian coordinates
X, X_T	hydrodynamic and thermal entry lengths (m)

Greek symbols

α, β	non-dimensional parameters
α_f	thermal diffusivity of the fluid (m^2/s)
Δ	variation
ϕ	area fraction
θ	angle of corrugation (rad)
κ	wall roughness (m)
μ	dynamic viscosity (kg/m s)
ν	kinematical viscosity (m^2/s)
ρ	density (kg/m^3)
$\bar{\rho}_c$	relative density of the core
ξ	rotated y coordinate

Non-dimensional groups

f	friction factor
Nu	Nusselt number
Pr	Prandtl number
Re	Reynolds number
Δ, Δ^*	geometric indices
Φ	fluid index
Π, Π^*	topological indices
Π_h	heat transfer parameter
Π_p	pumping power parameter

Subscripts and superscripts

0	upstream conditions
1	relative to one corrugated wall in the core
ave	averaged between the triangular and rhombic ducts
c	relative to the core
cond	conductive
conv	convective
cr	critical (for laminar to turbulent transition)
D	relative to the hydraulic diameter
f	relative to the fluid
H	relative to the core thickness
in	inlet
m	relative to the top metal face
max	maximum
out	outlet
rh	relative to the rhombic ducts
s	relative to the solid
tr	relative to the triangular ducts
T	thermal
w	relative to the fraction of the top face in direct contact with the fluid

approach has already been extensively used [3,8–17], here we account for the existence of two families of ducts (triangular and rhombic) with different flow regimes. Section 5 presents the genetic optimization scheme, the results are described in Section 6, and conclusions follow.

2. Background

A schematic of the panels under consideration, together with the coordinate system, is depicted in Fig. 1. When normalized by the panel length, L, four variables fully characterize the cellular geometry: the core thickness H_c/L, the core web thickness t/L, the corrugation angle θ and the order of corrugation n ($n = 1$ and 4, for the panels of Fig. 1). We envision a loading scenario wherein a uniform thermal flux Q is imposed on the top face. The bottom face and the sides are insulated, so that the flux is entirely removed by a cooling fluid. The fluid enters at a temperature $T_{f,in}$ and exits at a temperature $T_{f,out}$. The maximum temperature in the metal, $T_{m,max}$, occurs on the top face at the outlet.

To describe the flow characteristics, it is convenient to introduce three non-dimensional quantities: the Reynolds number Re_H, the friction factor f_H and the Nusselt number Nu_H. These parameters relate to the fluid velocity, the frictional dissipation, and the panel-level heat transfer coefficient h_H, respectively:

$$Re_H = \frac{\rho_f u_0 H_c}{\mu_f} \tag{1}$$

$$f_H = \frac{\frac{\Delta p}{L} H_c}{\frac{1}{2}\rho_f u_0^2} \tag{2}$$

$$Nu_H = \frac{h_H H_c}{k_f} = \frac{Q}{WL(T_m(x) - T_f(x))} \frac{H_c}{k_f} \tag{3}$$

where ρ_f, μ_f and k_f are the density, dynamic viscosity and thermal conductivity of the cooling fluid, Δp is the pressure drop over the entire length L of the panel, and u_0 is the

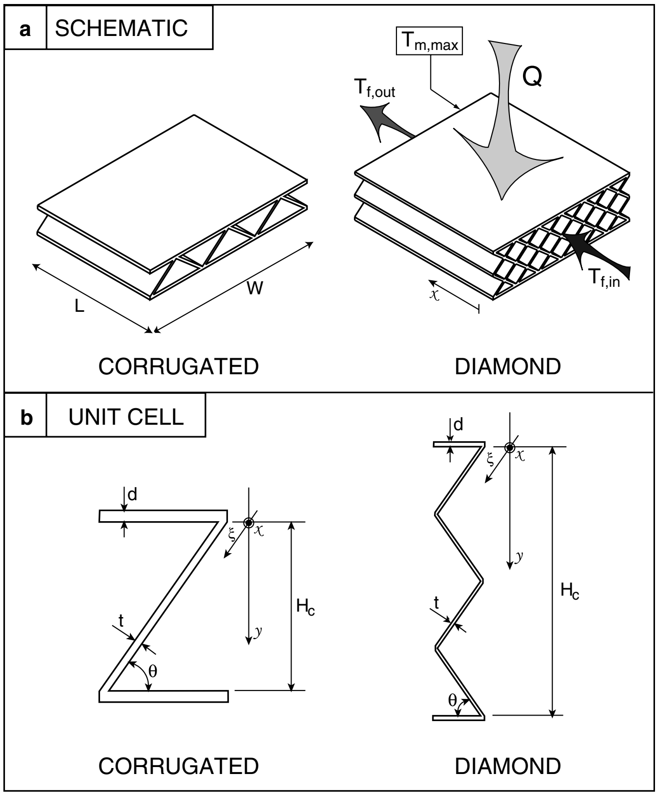

Fig. 1. (a) Schematic of the panels under consideration and thermal loading scenario; (b) unit cells for corrugated and diamond panels, with dimensions and coordinate system. The diamond panel sketched has order of corrugation $n = 4$.

mean fluid velocity *upstream* of the panel. The temperature $T_m(x)$ is the local value at the top face (averaged through the width of the panel, W), and $T_f(x)$ is the average (mixing-cup) temperature of the fluid, at axial location x. For fully developed flow, the temperature difference $T_m(x) - T_f(x)$ is independent of x, so that Eq. (3) defines the Nusselt number with no ambiguity [18]. Note that all the three quantities in Eqs. (1)–(3) have been normalized by the core thickness, thus allowing direct comparison of the active cooling performance for different designs [3].

Appropriate combinations of these three non-dimensional parameters can be used to identify the most promising designs for active cooling [3]. In particular, we can rearrange Eqs. (1)–(3) to express the results in terms of the pumping power P needed to maintain the fluid flow at a velocity u_0 against the pressure drop Δp:

$$\Delta p = \frac{1}{2}(f_H Re_H^2)\left(\frac{\mu_f^2}{\rho_f}\right)(LH_c^{-3}) \tag{4}$$

$$P = \Delta p u_0 W H_c = \frac{1}{2}(f_H Re_H^3)\left(\frac{\mu_f^3}{\rho_f^2}\right)(LWH_c^{-3}) \tag{5}$$

$$\frac{Q}{T_m(x) - T_f(x)} = (Nu_H)(k_f)(WLH_c^{-1}) \tag{6}$$

which, upon combining, give:

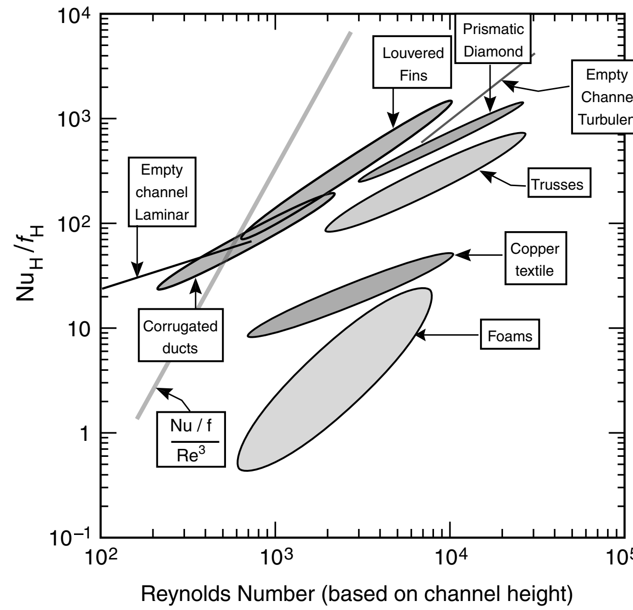

Fig. 2. Comparison of different heat sink technologies. The line of slope three is the index used to gain some preliminary information on the relative performance of different designs. Notice that this approach does not account for physical temperature limits in the heat sink itself.

$$\begin{aligned}
&\frac{Q}{(T_m(x) - T_f(x))P} = \Pi \cdot \Phi \cdot \Delta \\
&\Pi = \frac{Nu_H}{f_H Re_H^3} \\
&\Phi = \frac{k_f \rho_f^2}{\mu_f^3} \\
&\Delta = 2H_c^2
\end{aligned} \tag{7}$$

This formula reveals that the heat flux dissipated per unit temperature difference at a given pumping power can be expressed as the product of three terms: a non-dimensional topology index, Π, a fluid index, Φ, and a geometric index, Δ. For given panel thickness H_c and cooling fluid (Φ), optimizing the heat flux per unit temperature difference and pumping power is equivalent to maximizing Π. Identification of the best candidates is facilitated by maps plotting Nu_H/f_H against Re_H for several competing designs (Fig. 2), where contours of constant Π become lines of slope 3. Most of the ellipses in Fig. 2 are envelopes of experimental results (see [3] for details). Designs in the top left corner are the most efficient. According to this scheme, empty rectangular channels with laminar flow give the best thermal performance, while corrugated core panels are only as good as tetragonal and textile core panels and only slightly better than foam core panels. These conclusions are subject to a number of limitations addressed in the next section.

3. Problem statement

The preceding implications regarding the best thermal performance are misleading because of the following three fundamental limitations of the optimization scheme:

(a) No constraint was imposed on the maximum allowable temperature in the metal (or fluid). Consequently, at specified $T_m(x) - T_f(x)$, designs that are optimal at very low Reynolds number (empty ducts with laminar flow) reach higher temperatures than designs that operate in the turbulent flow range.
(b) The temperature difference $T_m(x) - T_f(x)$ is rarely a design parameter; usually the incoming fluid temperature, $T_{f,in}$, is specified by the system, while a constraint on the mechanical properties of the metal imposes a temperature maximum: $T_{m,out} = T_{m,max}$. A temperature difference $T_{m,max} - T_{f,in}$ is thus more useful, in practice.
(c) The preceding method assumes that the Reynolds number can be varied arbitrarily, and independently from Nu_H and f_H. This is not true, since the Reynolds number is related to the pumping power and the friction factor. Furthermore, the Reynolds number is not known a priori.

It follows from these limitations that a design-conscious optimization is required. Here we suggest an approach that addresses all of the above deficiencies. Specifically, we define a new objective function:

$$\frac{Q}{(T_{m,max} - T_{f,in})P} \tag{8}$$

Since two of the quantities in Eq. (8) should be known, the new method must be able to optimize the third. By invoking Eqs. (4)–(7), the objective function can be re-written as

$$\begin{aligned} \frac{Q}{(T_{m,max} - T_{f,in})P} &= \Pi^* \cdot \Phi \cdot \Delta^* \\ \Pi^* &= \frac{Nu_H (H_c/L)^2}{f_H Re_H^3 \left[1 + \frac{Nu_H}{Pr\, Re_H (H_c/L)}\right]} \\ \Delta^* &= 2L^2 \end{aligned} \tag{9}$$

where $Pr = \nu_f/\alpha_f = \mu_f c_p/k_f$ is the Prandtl number of the fluid.[1]

For any choice of coolant fluid and panel length, optimizing (8) translates into maximizing the non-dimensional parameter, Π^*.

In order to address the dependence on Reynolds number, we redefine the topology index as $\Pi^* = \Pi_h/\Pi_p$ where for every value of:

$$\Pi_p = \frac{f_H Re_H^3}{(H_c/L)^3} \tag{10}$$

we maximize:

$$\Pi_h = \frac{Nu_H}{(H_c/L)\left[1 + \frac{Nu_H}{Pr Re_H (H_c/L)}\right]} \tag{11}$$

[1] In deriving Eq. (9), we used the equalities: $T_{m,max} - T_{f,in} = (T_{m,max} - T_{f,out}) + \Delta T_f = (T_m(x) - T_f(x)) + \Delta T_f$; Eq. (27) was used to estimate ΔT_f.

Clearly, the problem has not changed, but now the two new topology indices relate to physical quantities:

$$\begin{aligned} \frac{Q}{T_{m,max} - T_{f,in}} &= k_f W \Pi_h \\ P &= \frac{1}{2}\frac{\mu_f^3}{\rho_f^2}\frac{W}{L^2}\Pi_p \end{aligned} \tag{12}$$

Maps of Π_h against Π_p will allow a meaningful comparison of different designs for the same working fluid, and will immediately identify the best candidates for active cooling at specified pumping power. In this article, we apply this method to prismatic core panels and seek geometric variables that maximize the heat transfer index for a wide range of the pumping power. An intermediate step relates the flow and thermal parameters for the panel (Re_H, f_H, Nu_H) to those for its constituents (the triangular and/or rhombic channels). The advantage is that correlations for channel-level friction factors and Nusselt numbers are widely available in the literature [19,20].

4. Transposing panel and channel-level indices

The approach used to calculate the friction factor differs in three ways from that used elsewhere [3,16,17]: (a) we use Π_p instead of Re_H (or u_0) as the independent variable, (b) we fully account for both laminar and turbulent flow, and (c) we recognize that a diamond core panel consists of both triangular and rhombic ducts (a distinction that becomes particularly important at low order of corrugation, n: see Fig. 1b). The calculation of the Nusselt number follows the method developed elsewhere [3,16,17], with the exception that the local heat transfer coefficient is averaged over triangular and rhombic ducts. Fully developed flow profiles (both kinematical and thermal) are implied, which requires that the panel be long enough to smooth out entry and exit effects (Appendix 1) [18]. The optima that are identified are only weakly dependent on temperature because the most temperature dependent index, Φ, is used outside the optimization algorithm. Accordingly, the temperature dependence of the properties is neglected: here all values have been calculated at 50 °C.

We assume that all channels (triangular close to the face sheets, and rhombic everywhere) are subjected to the same pressure drop: implying that the two families of channel shape experience different flow velocities (the faster flow being in the rhombic ducts by virtue of their larger hydraulic diameter). This assumption is clearly an idealization, but we believe it is more appropriate than assuming a uniform velocity profile and variable pressure drop.

Both the pressure drop and the flow velocities are unknown a priori, particularly whether the flow conditions are laminar or turbulent. Three options are possible: (a) laminar flow in both; (b) laminar flow in the triangular ducts and turbulent flow in rhombic channels; (c) turbulent flow in both. The protocol for addressing these options is addressed in Section 4.4.

4.1. Friction factor

The calculation of f_H and Re_H makes use of two conservation equations:

$$\frac{u_0}{1-\bar{\rho}_c} = \phi_{tr}u_{tr} + \phi_{rh}u_{rh} \quad \text{(mass conservation)} \tag{13}$$

$$P = \Delta p H_c W u_0 \quad \text{(momentum conservation)} \tag{14}$$

where u_{tr} and u_{rh} are the fully developed average fluid velocities within the triangular and rhombic channels, $\phi_{tr} = 1/n$ and $\phi_{rh} = 1 - 1/n$ are the area fractions of each family of channels, and $\bar{\rho}_c$ is the core relative density:

$$\bar{\rho}_c \approx 1 - \left[1 - \frac{n}{2\cos\theta}\frac{t}{H_c}\right]^2 \tag{15}$$

The channel-level Reynolds numbers are

$$Re_{tr} = \frac{\rho_f u_{tr} D_{tr}}{\mu_f}, \quad Re_{rh} = \frac{\rho_f u_{rh} D_{rh}}{\mu_f} \tag{16}$$

where D_{tr} and D_{rh} are the hydraulic diameters of the triangular and rhombic channels:

$$\begin{aligned} D_{tr} &= \frac{2\cos\theta}{1+\cos\theta}\left(\frac{H_c}{n} - \frac{t}{2\cos\theta}\right) \\ D_{rh} &= \frac{2\cos\theta}{n}H_c - t \end{aligned} \tag{17}$$

Eqs. (13) and (14) can be re-written in non-dimensional form as

$$\frac{Re_H}{1-\bar{\rho}_c} = \phi_{tr}\frac{Re_{tr}}{D_{tr}/H_c} + \phi_{rh}\frac{Re_{rh}}{D_{rh}/H_c} \quad \text{(mass conservation)} \tag{18}$$

$$\Pi_p = \frac{f_H Re_H^3}{(H_c/L)^3} \quad \text{(momentum conservation)} \tag{19}$$

By defining the channel-level friction factors as[2]:

$$f_{tr} = \frac{D_{tr}(\Delta p/L)}{2\rho_f u_{tr}^2}, \qquad f_{rh} = \frac{D_{rh}(\Delta p/L)}{2\rho_f u_{rh}^2} \tag{20}$$

the relations between channel-level and panel-level friction factors, in non-dimensional form, become

$$\begin{aligned} f_{tr} &= \frac{f_H}{4}\left(\frac{Re_H}{Re_{tr}}\right)^2\left(\frac{D_{tr}}{H_c}\right)^3 \\ f_{rh} &= \frac{f_H}{4}\left(\frac{Re_H}{Re_{rh}}\right)^2\left(\frac{D_{rh}}{H_c}\right)^3 \end{aligned} \tag{21}$$

By estimating f_{tr} and f_{rh} from correlations available in the literature (for laminar and turbulent flow), Eqs. (18), (19) and (21) enable the evaluation of f_H, Re_H, Re_{tr} and Re_{rh}. Hence we were able to relate flow properties at the individual channel level to macroscopic panel-level flow characteristics.

[2] The numerical factor differs from that in Eq. (2) [3] to be more consistent with the majority of the literature [18–20].

4.2. Nusselt number

The procedure for evaluating the Nusselt number involves the following four steps [3] (all coordinates are depicted in Fig. 1b):

(a) A unit cell, thickness H_c, is identified.
(b) The fluid temperature $T_f(x)$ is calculated by imposing energy conservation.
(c) An energy balance at the face-core interface is invoked to determine the heat flux entering the core.
(d) The temperature of the solid $T_s(x)$ within the unit cell is calculated as a function of $T_f(x)$ by using a one-dimensional fin analogy.

The channel-level Nusselt numbers,

$$Nu_{tr,rh} = \frac{h_{tr,rh}D_{tr,rh}}{k_f} = \frac{q(x,y,z)}{T_s(x,y,z) - T_f(x)} \tag{22}$$

are either found in the literature, or derived using experimental techniques or determined by numerical methods.

To proceed we adopt four simplifications:

(a) Conduction through the face is infinite (thin face approximation), so that its thickness does not appear in the problem.
(b) Axial conduction is negligible. While reasonable for the fluid, especially in the limit of large Peclet number [18], this assumption is more restrictive for the solid, particularly for thick walls and highly conductive materials. However, relaxing this hypothesis impedes an analytical derivation and severely complicates the ensuing optimization.
(c) The width of the panel W is large enough to eliminate edge effects such that all temperature distributions are functions of x and y only.
(d) The fluid temperature varies with x only; namely, $T_f(x)$ represents the mixing-cup temperature at location x.

With these simplifications, the temperature in the solid satisfies the one-dimensional fin equation:

$$\frac{\partial^2 T_s(x,\xi)}{\partial \xi^2} - \frac{2h}{k_s t}[T_s(x,\xi) - T_f(x)] = 0 \tag{23}$$

where $\xi = y/\sin\theta$ is the coordinate along the corrugated wall (see Fig. 1b), k_s is the thermal conductivity of the solid, and h is the local heat transfer coefficient (approximated as a weighted average of the triangular and rhombic channel values, $h = h_{tr}\phi_{tr} + h_{rh}\phi_{rh}$).

We solve (23), with boundary conditions:

$$\begin{cases} -k_s \left.\dfrac{\partial T_s}{\partial \xi}\right|_{\xi=0} = q_1 \\ \left.\dfrac{\partial T_s}{\partial \xi}\right|_{\xi=H_c/\sin\theta} = 0 \end{cases} \tag{24}$$

where q_1 is the heat flux entering the corrugated wall from one face (yet to be calculated). The resulting temperature in the solid is

$$T_s(x,\xi) = T_f(x) + \frac{q_1}{k_s m}\frac{\cosh(m(H_c/\sin\theta - \xi))}{\sinh(mH_c/\sin\theta)} \tag{25}$$

with $m = \sqrt{2h/k_s t}$.

The temperature in the fluid is readily calculated by imposing energy conservation along the x (axial) direction:

$$\dot{m}c_p\frac{dT_f(x)}{dx} = qW \tag{26}$$

Here q is the heat flux imposed on the top face sheet ($Q = qWL$), $\dot{m} = \rho_f u_0 W H_c$ is the mass flow rate, and c_p is the specific heat of the fluid. The solution is

$$T_f(x) = T_{f,in} + \frac{q}{H_c\rho_f c_p u_0}x. \tag{27}$$

In order to calculate q_1, we impose an energy balance at the node in contact with the top face:

$$q = q_w\phi_w + q_1(1-\phi_w) \tag{28}$$

where q_w is the heat flux into the fluid from the faces and $\phi_w \cong 1 - \bar{\rho}_c$ represents the area fraction of the face sheet in direct contact with the fluid. By noting that the heat flux from the faces is

$$q_w(x) = h_{tr}[T_s(x,\xi=0) - T_f(x)] = \frac{h_{tr}q_1}{k_s m}\tanh^{-1}(mH_c/\sin\theta) \tag{29}$$

we can express q_1 as a function of q. By recalling the definition of Nusselt number at the panel level (Eq. (3)), and analogously defining the Nusselt numbers at the cell level:

$$Nu_{tr} = \frac{h_{tr}D_{tr}}{k_f}, \qquad Nu_{rh} = \frac{h_{rh}D_{rh}}{k_f} \tag{30}$$

we can finally write:

$$Nu_H = \frac{Nu_{tr}}{D_{tr}/H_c}(1-\bar{\rho}_c) + \bar{\rho}_c \times\sqrt{2\frac{k_s}{k_f}\left(\frac{Nu_{tr}}{D_{tr}/H_c}\phi_{tr} + \frac{Nu_{rh}}{D_{rh}/H_c}\phi_{rh}\right)\frac{H_c/L}{t/L}} \cdot \tanh\left[\sqrt{2\frac{k_f}{k_s}\left(\frac{Nu_{tr}}{D_{tr}/H_c}\phi_{tr} + \frac{Nu_{rh}}{D_{rh}/H_c}\phi_{rh}\right)\frac{H_c/L}{t/L}}\csc\theta\right] \tag{31}$$

This result allows the overall thermal characteristics to be related to the Nusselt numbers evaluated at the cell level: Nu_{tr} and Nu_{rh}.

4.3. Correlations at the channel level

Correlations are available in the literature for laminar and turbulent flow in ducts [19,20]. For *laminar flow*, Nu only depends on the shape of the channel and is independent of Re, whereas f is inversely proportional to Re. For *turbulent flow*, Nu increases with Re (at a rate that depends on the correlation used); whereas f, in the rough channel limit [18], only depends on the ratio of the channel roughness to the hydraulic diameter (κ/D). The details are reported in Table 1, with the angular dependences of Nu and ($f \cdot Re$) in the laminar regime plotted in Fig. 3.

4.4. Heat transfer and pumping power parameters

Since the Reynolds numbers are not known a priori, it cannot be ascertained whether the flow is laminar or turbulent, which prevents direct determination of the panel-level friction factor. The iterative scheme illustrated on Fig. 4 is invoked. Three possibilities must be pursued:

The flow is laminar in both ducts, whereupon

$$f_H = \frac{\alpha}{Re_H} \quad \text{and} \quad Re_H = \sqrt{\frac{\Pi_p(H_c/L)^3}{\alpha}} \tag{32}$$

with

$$\alpha = \frac{4}{1-\bar{\rho}_c}\Bigg/\left(\phi_{tr}\frac{(D_{tr}/H_c)^2}{(f_{tr}\cdot Re_{tr})} + \phi_{rh}\frac{(D_{rh}/H_c)^2}{(f_{rh}\cdot Re_{rh})}\right) \tag{33}$$

The duct level Reynolds numbers follow as

$$Re_{tr} = \frac{\alpha(D_{tr}/H_c)^3 Re_H}{4(f_{tr}\cdot Re_{tr})} \quad \text{and} \quad Re_{rh} = \frac{\alpha(D_{rh}/H_c)^3 Re_H}{4(f_{rh}\cdot Re_{rh})} \tag{34}$$

If any local Re calculated according to these equations exceeds the turbulent transition ($Re_{crit} = 2000$ for the calculations here), the flow is assumed not to be laminar in both channels.

The flow is turbulent in both ducts, whereupon

$$f_H = \left[(1-\bar{\rho}_c)\left(\phi_{tr}\sqrt{\frac{D_{tr}/H_c}{4f_{tr}}} + \phi_{rh}\sqrt{\frac{D_{rh}/H_c}{4f_{rh}}}\right)\right]^{-2} \tag{35}$$

Table 1
Summary of correlations used

	Nusselt number		Friction factor	
	Laminar†	Turbulent*	Laminar†	Turbulent*
Triangular ducts	$Nu_{tr}(\theta)$	$\frac{(f_{tr}/2)(Re_{tr}-1000)Pr}{1+12.7\sqrt{f_{tr}/2}(Pr^{2/3}-1)}$	$(f_{tr}\cdot Re_{tr})(\theta)$	$\left(1.74\log\left(\frac{D_{tr}}{\kappa}\right)+2.78\right)^{-2}$
Rhombic ducts	$Nu_{rh}(\theta)$	$\frac{(f_{rh}/2)(Re_{rh}-1000)Pr}{1+12.7\sqrt{f_{rh}/2}(Pr^{2/3}-1)}$	$(f_{rh}\cdot Re_{rh})(\theta)$	$\left(1.74\log\left(\frac{D_{rh}}{\kappa}\right)+2.78\right)^{-2}$

The functions $Nu_{tr}(\theta)$, $Nu_{rh}(\theta)$, $(f_{tr}\cdot Re_{tr})(\theta)$ and $(f_{rh}\cdot Re_{rh})(\theta)$ are plotted in Fig. 3.
* From [18].
† From [19].

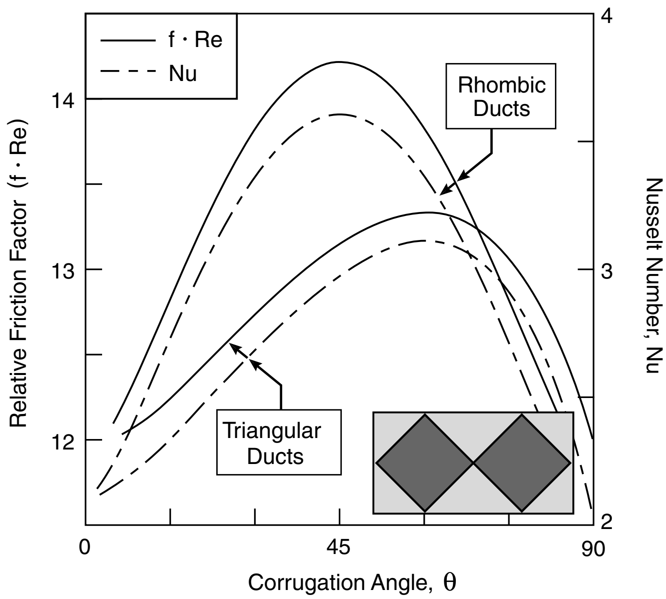

Fig. 3. Plot of the correlations used for the channel-level Nusselt numbers and friction factors for triangular and rhombic channels as a function of the corrugation angle. H1 boundary conditions were assumed (uniform temperature peripherally, and uniform heat flux axially). The data were obtained from [19].

The panel-level Reynolds number will then be $Re_H = (\Pi_p/f_H)^{1/3} H_c/L$, and the local Reynolds numbers at the duct level will be

$$Re_{tr} = \sqrt{\frac{(D_{tr}/H_c)^3}{4f_{tr}} f_H Re_H} \quad \text{and}$$

$$Re_{rh} = \sqrt{\frac{(D_{rh}/H_c)^3}{4f_{rh}} f_H Re_H} \tag{36}$$

If $Re_{tr} < Re_{crit}$, *the flow will be laminar in the triangular channels, but turbulent in the rhombic*. In this case, the friction factor can be obtained by numerically solving:

$$\phi_{tr}(1-\bar{\rho}_c)\frac{(D_{tr}/H_c)^2}{4(f_{tr}\cdot Re_{tr})}\sqrt[3]{\frac{\Pi_p}{f_H}\frac{H_c}{L}}f_H + \phi_{rh}(1-\bar{\rho}_c)\sqrt{\frac{D_{rh}/H_c}{4f_{rh}}f_H} = 1 \tag{37}$$

Once the friction factor is obtained, the panel-level and duct-level Re become:

$$Re_H = \sqrt[3]{\frac{\Pi_p}{f_H}\frac{H_c}{L}}, \quad Re_{tr} = \frac{f_H Re_H^2}{4(f_{tr}\cdot Re_{tr})}\left(\frac{D_{tr}}{H_c}\right)^3,$$

$$Re_{rh} = \sqrt{\frac{(D_{rh}/H_c)^3}{4f_{rh}} f_H Re_H} \tag{38}$$

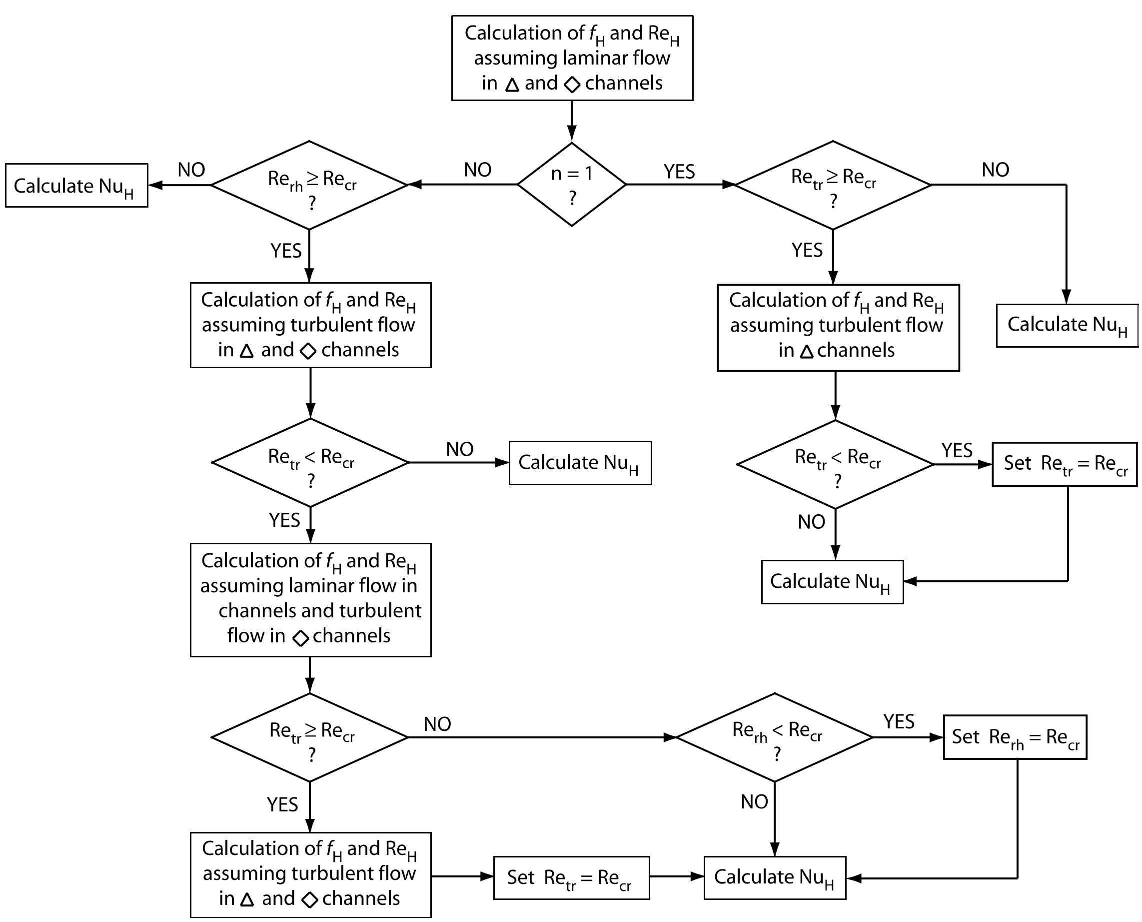

Fig. 4. Flowchart of the procedure used in the calculation of panel-level friction factor and Nusselt number. This scheme is necessary since the flow conditions (laminar or turbulent flow) are not known a priori.

Table 2
Properties of the fluids and metals considered [18]. All fluid properties are at 323 K (50 C)

	$k_{f,s}$ (W/m K)	μ_f (kg/m s)	ρ_f (kg/m^3)	ν_f (m^2/s)	Pr	$k_f\rho_f^2/\mu_f^3$ (K^{-1} m^{-2})
Air	0.028	2.00×10^{-5}	1.06	1.89×10^{-5}	0.70	3.93×10^{12}
Water	0.64	5.48×10^{-4}	988	5.55×10^{-7}	3.57	3.80×10^{15}
Gasoline	0.11	3.70×10^{-4}	721	5.13×10^{-7}	7.40	1.13×10^{15}
Aluminum	200					
Titanium	22					

The approach taken here is expected to be most inaccurate when $Re \approx Re_{crit}$ in either of the channel types, since the correlations used do not capture the details of the transition.

5. The thermal optimization scheme

Four different materials systems have been analyzed: aluminum-air, aluminum-water, aluminum-gasoline and titanium-gasoline. The relevant materials properties are reported in Table 2. As already noted, variations in properties with temperature have been ignored: values at 50 °C were used. The optimization scheme proceeds as follows:

(a) Bounds for the geometric variables are defined:

$$\begin{aligned}&0.005 \leqslant \frac{H_c}{L} \leqslant 0.1\\&0.0005 \leqslant \frac{t}{L} \leqslant 0.01\\&25^\circ \leqslant \theta \leqslant 75^\circ\\&1 \leqslant n \leqslant 33\end{aligned} \tag{39}$$

(b) A reasonable range for the pumping power coefficient is chosen ($10^{12} \leqslant \Pi_p \leqslant 10^{22}$) to assure that for all the fluids considered (air, water and gasoline) and for 1 m panels, the range of powers 1 W → 100 kW are incorporated.

(c) An upper bound for the core density is specified; for most calculations, $\bar{\rho}_c \leqslant 0.5$.The roughness of the core webs is assumed to scale with the core web thickness t/L; in our calculations we take: $\kappa/t = 0.05$.

(d) A genetic optimization method was used for all the calculations (see Appendix 3 for details). The geometry of each material system was optimized to obtain the maximum heat transfer parameter using many values of the pumping power parameter (1024 values in the aforementioned interval).

6. Optimal designs

6.1. Thermal performance

The thermal performance, $\Pi_h(\Pi_p)$ of the fully optimized panel with $\bar{\rho}_c \leqslant 0.5$ is plotted in Fig. 5, superimposed on the optimal performances of panels chosen for their ease of fabrication, as well as their close connection with structural optima [1,2]:

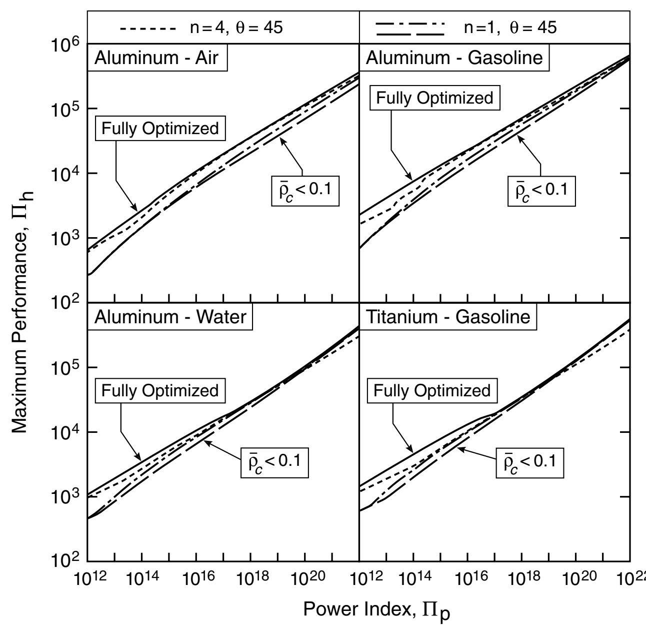

Fig. 5. Optimal thermal performance as a function of pumping power for the four materials systems under investigation. Results are presented for the fully optimized geometry, as well as for three more restrictive cases: (a) $\theta = 45°$, $n = 4$, (b) $\theta = 45°$, $n = 1$, and (c) $\theta = 45°$, $n = 1$ with $\bar{\rho}_c \leqslant 0.1$. Except for case (c), all core densities are constrained to $\bar{\rho}_c \leqslant 0.5$.

(a) $\theta = 45°$, $n = 4$, (b) $\theta = 45°$, $n = 1$, and (c) $\theta = 45°$, $n = 1$ with $\bar{\rho}_c \leqslant 0.1$. The *major finding is that these constraints have minimal effect on the optimal thermal performance*. In particular, case (a) is almost identical to the fully optimized panel, except at very low pumping power.

Inspection of the results for the fully optimized designs reveals several important characteristics:

(i) The optimal angles are almost always close to either of the bounds, $\theta = 25°$ or $\theta = 75°$. Since imposing $\theta = 45°$ does not reduce the performance significantly, this suggests that the angle can be set arbitrarily to obtain near-optimal designs.

(ii) The order of corrugation has a more pronounced effect. For $\theta = 45°$, among values in the range $1 \leqslant n \leqslant 16$, n=4 is optimal.

(iii) The optimal densities are quite high, $\bar{\rho}_c > 0.15$, often saturating at $\bar{\rho}_c \approx 0.5$.

The similarity of the optimal performances of the designs studied does not suggest that the thermal performance is geometry insensitive. Changing one geometric variable and leaving the others unchanged has a dramatic effect on the performance. This aspect of performance can be inferred from Figs. 6–8, where the optimal values of core thickness (H_c/L) and core web thickness (t/L) are presented. Note that imposing constraints on some geometric variables (n and θ) substantially modifies the optimum for the others. Some of the factors affecting the preferred geometries are elaborated below.

6.2. Topology

The two heat transfer mechanisms present in cellular panels (conduction through the core webs and convection in the fluid) impose opposite requirements on the geometric variables. Efficient conduction requires large core web thickness and small panel thickness, resulting in small temperature difference between metal and fluid (see Eq. (25)). Conversely, convection is enhanced by a large panel thickness (at least a large pumping power), resulting in large hydraulic diameters. It follows that the optimal geometries resulting from this trade-off are difficult to rationalize from simple physical arguments.

Optimal values of $\bar{\rho}_c$, H_c/L and t/L are reported in Figs. 6–8. For the preferred geometries, the results fluctuate at low pumping power due to laminar-to-turbulent transitions (at low power the optimal conditions are laminar, but they gradually transition to turbulent). The procedure for capturing this transition in the model (see Fig. 4) is responsible for the oscillations in the figures. The issues are illustrated for the case $\theta = 45°$, $n = 4$ for the aluminum-water system.

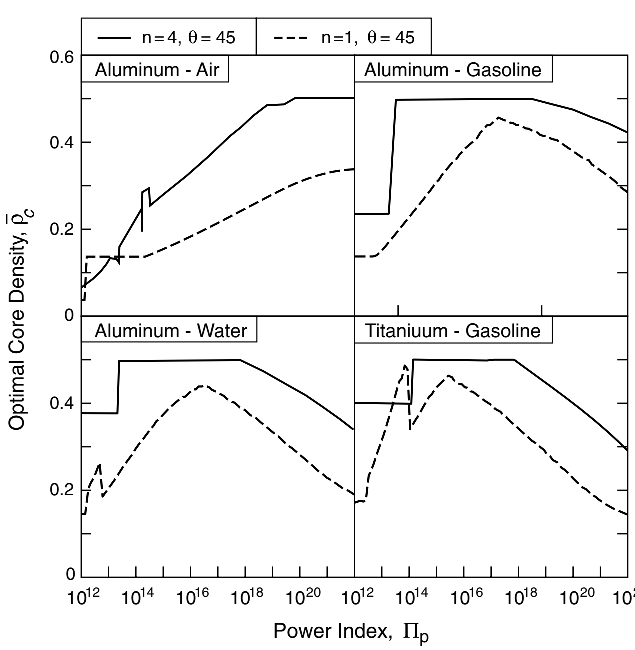

Fig. 6. Optimal core densities for the panel designs (a) $\theta = 45°$, $n = 4$ and (b) $\theta = 45°$, $n = 1$. The density was constrained to $\bar{\rho}_c \leqslant 0.5$.

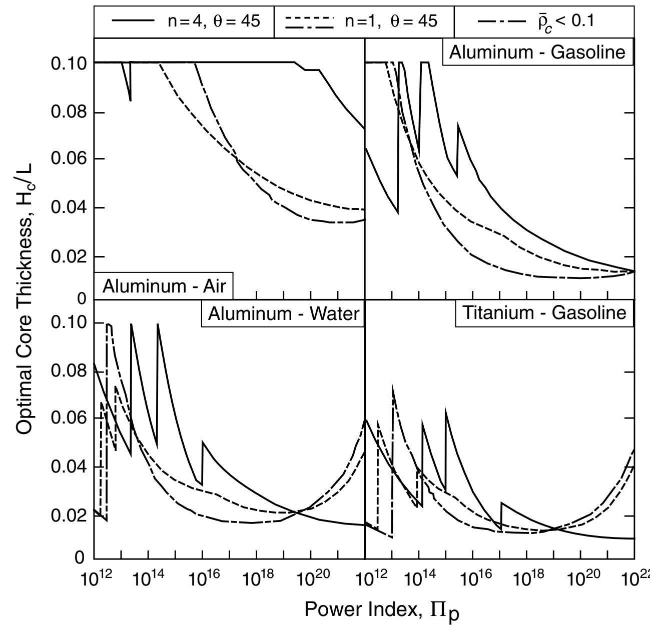

Fig. 7. Optimal core thickness for the panel designs (a), (b) and (c) (see caption to Fig. 5). The spikes in some curves are due to laminar to turbulent transitions in the optimal flow conditions. For the case $n = 4$, the optimal dimensions between the second and the third spike are related to the details of the model used to capture transition (see Fig. 4). Except for case (c), all core densities are constrained to $\bar{\rho}_c \leqslant 0.5$.

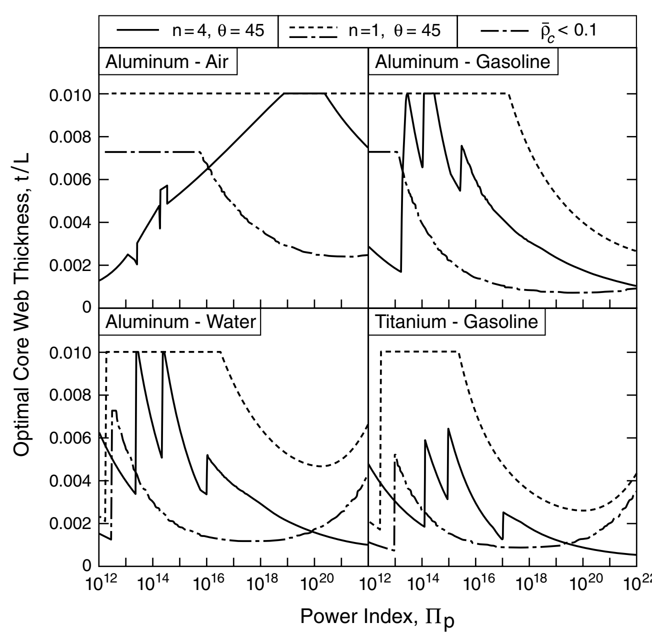

Fig. 8. Optimal core web thickness for the panel designs (a), (b) and (c) (see caption to Fig. 5). Except for case (c), all core densities are constrained to $\bar{\rho}_c \leqslant 0.5$.

At lowest power, both H_c/L and t/L decrease with Π_p, and the flow is laminar in both channels. The first spike corresponds to the transition $Re \rightarrow Re_{cr}$ in the rhombic channels. At this stage, the optimal dimensions decrease abruptly by maintaining $Re_{rh} \cong Re_{crit} = 2000$. When the transition is complete in the rhombic channels another abrupt change occurs. Thereafter, the dimensions again decrease until the flow in the triangular channels becomes turbulent (third spike). It follows that, in this range, the optimal dimensions are dependent on the approach used for capturing transition in the model.

Doubts about the validity of this model might arise when most of the flows are laminar or transitional. In fact, under these conditions, the optimal core thickness becomes large (Fig. 7) and the best performance occurs at low order of corrugation. The confluence of these two effects causes the flow to be in a developing mode over most of the panel (see Appendix 1), thus violating a key assumption. When the model is used in such conditions, care should be taken to ensure the hypotheses are not violated. This is a particular problem at the micro-scale. Referring to Eq. (12), if W and L become proportionally smaller, then the ratio W/L^2 becomes large. Thus, even if P is kept constant (in fact, it is likely to decrease as length-scales get smaller), Π_p decreases and the optimal flow is laminar.

6.3. Material trends

The four plots in Fig. 5 reveal effects of the material properties. Only two are needed to characterize the system: the Prandtl number of the fluid (Pr) and the ratio of the conductivities of solid to fluid. Comparing the aluminum-gasoline and titanium-gasoline systems, we note that the 10-fold increase in the conductivity ratio yields only a marginal benefit in the thermal performance: a synopsis of this phenomenon is provided in Appendix 2. Similarly, a comparison of the systems aluminum-air and aluminum-water reveals that a 50-fold increase in Pr from air to water (0.7–3.57) more than compensates a 23-fold decrease in the conductivity ratio (from 7000 to 300). Consequently, the aluminum-water system has superior performance.

A more relevant comparison is obtained by plotting the heat dissipation parameter $Q/(T_{\mathrm{m,max}} - T_{\mathrm{f,in}})W$ against the pumping power parameter PL^2/W (Fig. 9), which incorporates the effect of the fluid property parameter Φ. This comparison reveals that exchanging air for water provides nearly two orders of magnitude benefit, demonstrating that Φ is the most influential material parameter.

6.4. Thermo-structural designs

The large core densities for optimal active cooling are far from the structural optimum [1]. To illustrate the consequences, we use gasoline as the cooling medium. From a structural perspective, in the transverse direction, $n = 4$ is the preferred order of corrugation, whereas $n = 1$ is preferable for longitudinal loads [1]. The heat transfer performance of these two panels, optimized for minimum weight under flexural loads, are plotted as a function of the loading parameter V^2/EM on Fig. 10, for a wide range of pumping power parameter. It is apparent that the structurally optimized panels have appreciably diminished thermal performance, relative to their thermally optimized counterparts. Note, however, that, for some panels, the reduction from optimality is small: less than a factor two.

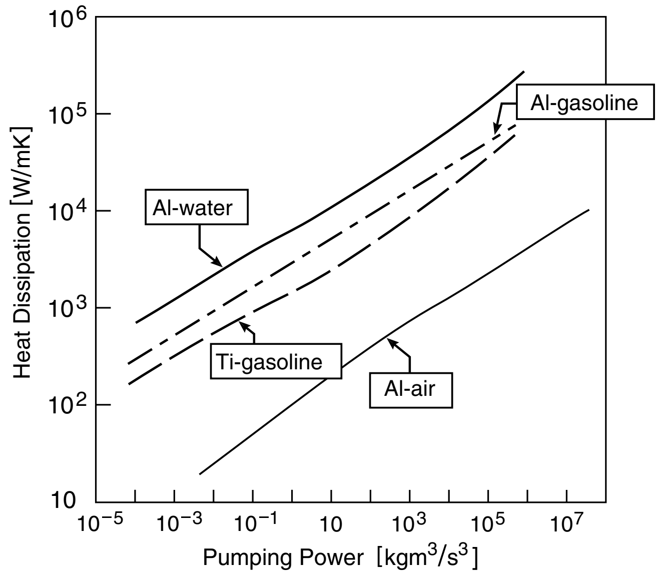

Fig. 9. Optimal thermal performance for the fully optimized panels plotted in dimensional coordinates ($Q/(T_{\mathrm{m,max}} - T_{\mathrm{f,in}})$ 1pt W against PL^2/W) to emphasize the effect of materials properties. The key materials parameter of the cooling medium is $k_\mathrm{f}\rho_\mathrm{f}^2/\mu_\mathrm{f}^3$: the higher, the better.

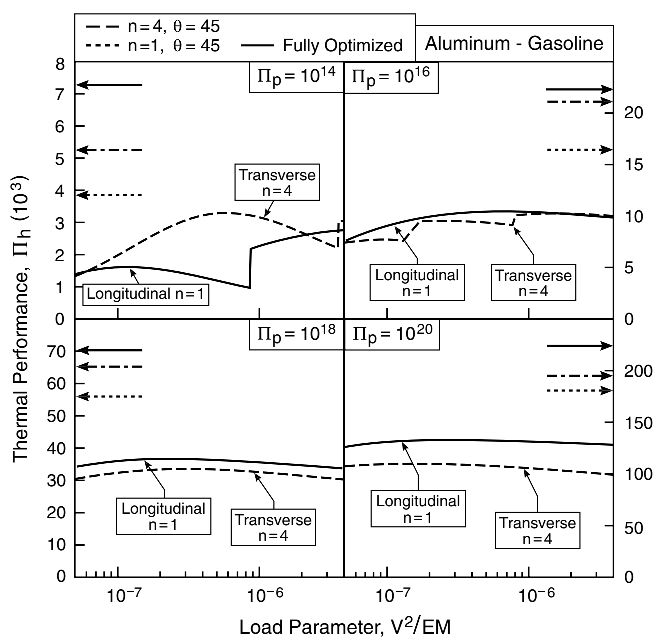

Fig. 10. Active cooling performance of structurally optimized panels (from [1]), as a function of the loading parameter, V^2/EM, for the system aluminum-gasoline; optimal dimensions pertinent to three-point bending loads were used. Two panels are considered: corrugated core panels ($n = 1$) optimized for longitudinal loadings, and diamond core panels ($n = 4$) optimize for transverse loadings ($\theta = 45°$ in both cases). Thermally optimized panels are superimposed for comparison.

7. Conclusions

Geometric optimization of prismatic panels with corrugated and diamond cores has been performed with the goal of maximizing their active cooling performance. We have presented an approach having the attribute that it incorporates physical quantities of primary relevance to design optimization, while still retaining generality through non-dimensional groups. Two new non-dimensional parameters reduce the number of free variables, while retaining a clear connection with physical quantities of interest, namely the pumping power, the dissipated heat flux, the inlet fluid temperature and the maximum temperature in the panel.

Prior analytical methods [3,16,17] have been extended to account for the presence of two geometrically different families (triangular near the faces and rhombic elsewhere), which experience different flow conditions (laminar or turbulent). Since neither the inlet flow velocity nor the pressure drop are known a priori, instead, the pumping power is used as the imposed quantity.

A genetic algorithm has been used to find the geometries that maximize the heat transfer parameter at various levels of the pumping power; four different material systems were analyzed (aluminum-air, aluminum-water, aluminum-gasoline and titanium-gasoline). The most important fluid property emerges as $k_f\rho_f^2/\mu_f^3$: the optimal cooling medium maximizes this quantity. The analysis revealed that the geometry can be optimized for a wide range of the order of corrugation (the number of straight core segments per unit cell) and corrugation angle without much detriment in thermal performance. These findings provide considerable geometric flexibility when attempting combined thermal and structural optimization. In some situations, structurally optimized geometries provide active cooling performances within a factor two of thermally optimized panels.

Acknowledgement

This work was supported by the ONR through a MURI program on Revolutionary Materials for Hypersonic Flight (Contract No. N00014-05-1-0439).

Appendix 1. Summary of conditions leading to fully developed flow profiles [18]

For *laminar* flow, the kinematical and thermal entry lengths, X and X_T respectively, in a duct with hydraulic diameter D are given by

$$\begin{aligned} X &\approx 0.026 Re_D D \\ X_T &\approx Pr X \end{aligned} \tag{A.1}$$

where $Re_D = \rho_f u D/\mu_f$, with u the average flow velocity in the duct.

For *turbulent* flow, the two entry lengths are similar to each other, and much shorter than in the laminar case:

$$X \approx X_T \approx 10D \tag{A.2}$$

Appendix 2. The role of the thermal conductivity of the solid

The ratio of the solid to the fluid thermal conductivity, embedded in the heat transfer index (Eq. (11)), is intimately related to the geometric parameters. A qualitative argument on its effect can be presented as follows.

In the geometries considered, heat is transferred down the core by conduction and released to the fluid via convection. The thermal resistance associated with conduction scales as $R_{\text{cond}} \sim 1/k_s$, whereas the convective resistance scales as $R_{\text{conv}} \sim 1/h \sim 1/k_f$.[3]

Since the principle in heat transfer enhancement is to reduce the highest thermal resistance, improving the solid conductivity will help only in situations where $R_{\text{cond}} > R_{\text{conv}}$.

A more quantitative assessment can be given for *fixed fluid properties*.

For any given fluid, maximizing the heat transfer performance of the structure is equivalent to maximizing the panel-level Nusselt number (see Eq. (3)). This is the sum of two terms (Eq. (31)): the first scales with $1-\bar{\rho}_c$, due to convection from the faces into the fluid, whereas the second scales with $\bar{\rho}_c$, and expresses the contribution from the core to the overall heat sink performance. We can re-write this core contribution as

$$Nu_H^{\text{core}} = \bar{\rho}_c \beta \sqrt{k_s/k_f} \tanh\left(\frac{\beta}{\sqrt{k_s/k_f}\sin\theta}\right) \tag{A.3}$$

where $\beta = \sqrt{2Nu_{\text{avg}}H_c/t}$, and $Nu_{\text{avg}} = \frac{Nu_{\text{tr}}}{D_{\text{tr}}/H_c}\phi_{\text{tr}} + \frac{Nu_{\text{rh}}}{D_{\text{rh}}/H_c}\phi_{\text{rh}}$.

For laminar flow, the parameter β is only a function of the panel geometry, whereas for turbulent flow it also depends on the Prandtl number of the fluid (see Table 1).

If we estimate the order of magnitude of β (using the correlations presented in Section 3.3), we can plot the core performance against the conductivity ratio (Fig. A1). Notice that a high value of β implies a low convective resistance, and as a result, increasing the solid conductivity has a significant effect; conversely, at low β the convective resistance is high, and the effect of the solid conductivity saturates. For gasoline, changing from aluminum to titanium (an order of magnitude increase in the conductivity) increases the core performance by less than a factor 3 at high β but only 30% at low β.

It is worth mentioning that these conclusions only hold true at fixed fluid properties, since the thermal performance depends on k_f and k_s separately, and not only on the conductivity ratio.

[3] By virtue of the non-slip hypothesis, heat is transferred by pure conduction from the solid to the first layer of motionless fluid near the wall, resulting in $h = k_f(\partial T_f/\partial\eta)|_{\eta=0}/(T_w - T_f)$, where η is the coordinate normal to the core web.

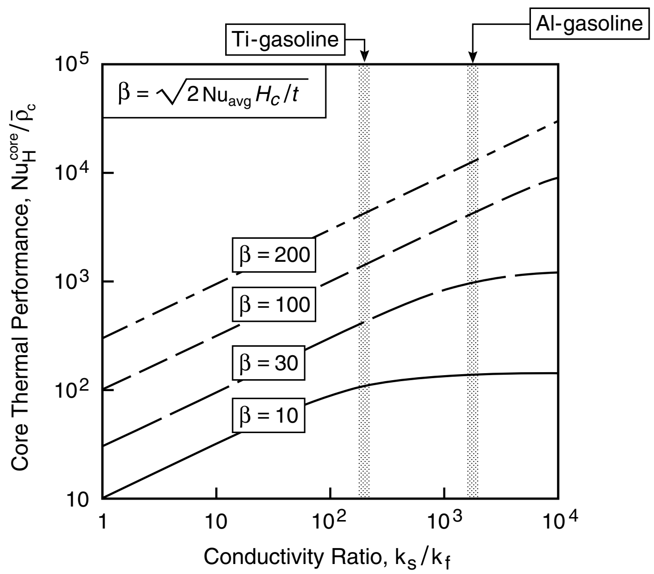

Fig. A1. Core contribution to the thermal performance as a function of the solid to fluid conductivity ratio at fixed fluid properties. The position of two of the systems studied is superimposed on the plot. Notice that (i) the performance scales non-linearly with the conductivity ratio, and (ii) for low values of β the benefit saturates at high conductivity ratio.

Appendix 3. The genetic algorithm

A genetic algorithm [21,22] was coded and used for all optimizations. The real-coded version was preferred over the more popular binary-coded version, for its ease of implementation and fast convergence. The ranges of the four optimization variables were divided into sub-intervals (2^{20} for H_c/L and t/L, 2^9 for θ and 2^5 for n); with the end points of each uniquely associated with an integer (between 1 and the number of sub-intervals for that variable). In this algorithm, each of these 4 numbers is a *gene*, so that each completely expresses a variable. Chromosomes were formed as vectors of 4 genes. A random population of 6000 chromosomes was initially created. The *fitness* of each chromosome (i.e. the value of the thermal parameter) was calculated and the population sorted in decreasing order of fitness. The best 20–40 chromosomes were retained (*elitism*), whereas the others were combined (two-by-two) in accordance with a set of rules to generate a new population (*crossover*). A combination of three crossover strategies was used to generate the *child* chromosomes: *one-point* (all genes of the two parents are exchanged after a random position), *two-point* (all the genes of the two parents are exchanged between two random positions) and *weighed average* (all the genes of the child chromosome were created as some weighed average of the genes of its parents). A small fraction of the new population (5%) was randomly modified (*mutation*) to allow the algorithm to sample a wide search space. This process was repeated for 30 times. After a convergence check, the best chromosome was chosen as the optimal.

The performance of the optimizer (its ability to converge to the global maximum) was tested against a brute-force scheme, consisting of evaluating of the function at a large series of discrete points and manually choosing the maximum. The agreement was excellent in all cases.

References

[1] L. Valdevit, J.W. Hutchinson, A.G. Evans, Structurally optimized sandwich panels with prismatic cores, Int. J. Solids Struct. 41 (2004) 5105–5124.
[2] L. Valdevit, Z. Wei, C. Mercer, F. Zok, A.G. Evans, Structural performance of near-optimal sandwich panels with corrugated cores, Int. J. Solids Struct., in press.
[3] T.J. Lu, L. Valdevit, A.G. Evans, Active cooling by metallic sandwich structures with periodic cores, Prog. Mater. Sci. 50 (2005) 789–815.
[4] N. Wicks, J.W. Hutchinson, Optimal truss plates, Int. J. Solids Struct. 38 (2001) 5165–5183.
[5] N. Wicks, J.W. Hutchinson, Performance of sandwich plates with truss cores, Mech. Mater. 36 (2004) 739–751.
[6] A.G. Evans, J.W. Hutchinson, N.A. Fleck, M.F. Ashby, H.N.G. Wadley, The topological design of multifunctional cellular metals, Prog. Mater. Sci. 46 (2001) 309–327.
[7] H.J. Rathbun, F.W. Zok, A.G. Evans, Strength optimization of metallic sandwich panels subject to bending, Int. J. Solids Struct. 42 (2005) 6643–6661.
[8] T.J. Lu, H.A. Stone, M.F. Ashby, Heat transfer in open-cell metal foams, Acta Mater. 46 (1998) 3619–3635.
[9] S.Y. Kim, B.H. Kang, J.H. Kim, Forced convection from aluminum foams in an asymmetrically heated channel, Int. J. Heat Mass Transfer 44 (2001) 1451–1454.
[10] T. Kim, C.Y. Zhao, H.P. Hodson, T.J. Lu, Convective heat dissipation with lattice-frame materials, Mech. Mater. 36 (2004) 1011–1020.
[11] T. Kim, H.P. Hodson, T.J. Lu, Fluid-flow and heat-transfer in untralightweight lattice-frame materials, Int. J. Heat Mass Transfer 47 (2004) 1129–1140.
[12] T. Kim, H.P. Hodson, T.J. Lu, Pressure loss and heat transfer mechanisms in a lattice-frame structured heat exchanger, J. Mech. Eng. Sci. 218 (2004) 1321–1336.
[13] F. Hoffmann, T.J. Lu, H.P. Hodson, Heat transfer performance of Kagome structures, Paper HX07, in: 8th UK National Heat Transfer Conference, Oxford, 9–10 September 2003.
[14] J. Tian, T. Kim, T.J. Lu, H.P. Hodson, D.T. Queheillalt, H.N.G. Wadley, The effects of topology upon fluid-flow and heat-transfer within cellular copper structures, Int. J. Heat Mass Transfer 47 (2004) 3171–3186.
[15] J. Tian, T.J. Lu, H.P. Hodson, D.T. Queheillalt, H.N.G. Wadley, Thermal-hydraulic performance of sandwich structures with wire mesh cores and embedded heat pipes, in: 13th International Heat Pipe Conference, Shanghai, China, 21–25 September 2004.
[16] T.J. Lu, Heat transfer efficiency of metal honeycombs, Int. J. Heat Mass Transfer 42 (1999) 2031–2040.
[17] S. Gu, T.J. Lu, A.G. Evans, On the design of two-dimensional cellular metals for combined heat dissipation and structural load capacity, Int. J. Heat Mass Transfer 44 (2001) 2163–2175.
[18] A. Bejan, Convection Heat Transfer, 2nd ed., Wiley, New York, 1995.
[19] R.K. Shah, A.L. London, Laminar flow forced convection in ducts, in: T.F. IrvineJr., J.P. Hartnett (Eds.), Advances in Heat Transfer, Academic Press, 1978.
[20] M.S. Bhatti, R.K. Shah, Turbulent and transition flow convective heat transfer in ducts, in: S. Kakac, R.K. Shah, W. Aung (Eds.), Handbook of Single-Phase Convective Heat Transfer, Wiley, New York, 1987, Chap. 4.
[21] M. Michell, An Introduction to Genetic Algorithms, MIT Press, 1998.
[22] D.S. Weile, E. Michielssen, Genetic algorithm optimization applied to electromagnetics: A review, IEEE Trans. Antenn. Propag. 45 (1997) 343–353.